ME525 Applied Acoustics Lecture 23, Winter 2024
Method of Normal Modes

Peter H. Dahl, University of Washington

Normal Modes

The method of images yields a "theoretical" exact solution to the problem of a point source within a waveguide, with upper boundary condition (at $z = 0$) of $p(0) = 0$, and lower boundary condition (at $z = H$) of $\frac{\partial p}{\partial z}(H) = 0$–provided enough images are used to reach a degree of convergence.

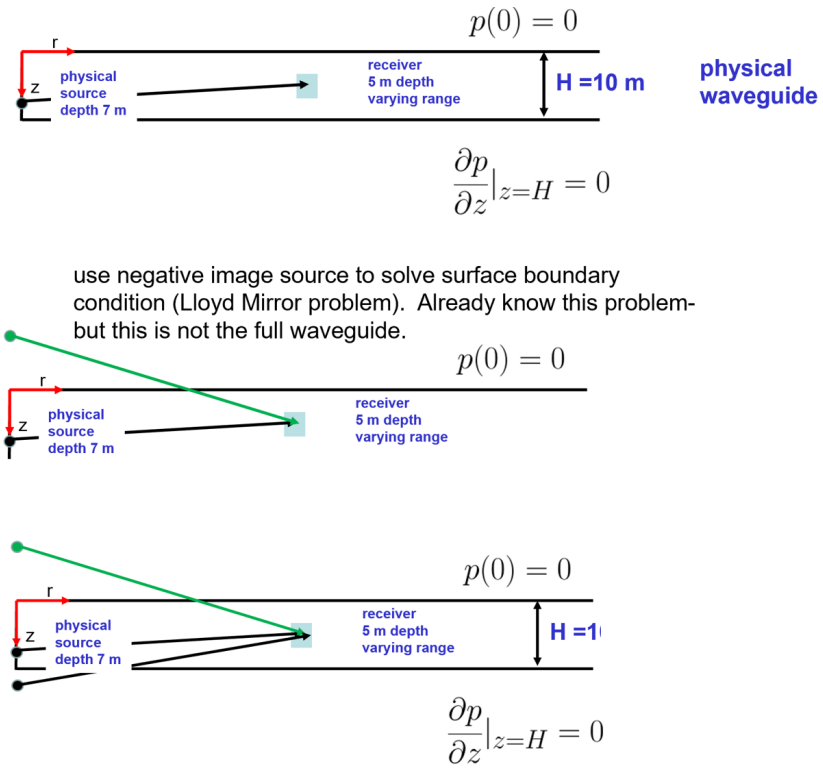

Figure 1: An apparent problem with the method of images once two boundaries at $z = 0, H$ introduced.

The negative image source above the $z = 0$ boundary combines with true source within the waveguide to satisfy the boundary condition at $z = 0$, and the positive image below the $z = H$ boundary combines with the true source to satisfy the boundary condition a $z = H$. However the true source plus positive image now require a second negative image source to satisfy boundary

condition at $z = 0$. The process of balancing out positive and negative image sources continues on to infinity or until some degree of convergence is reached.

This solution is from Frisk (Eq. 4.82, p. 83). It's relatively easy to code up, though care is needed to keep track of the expanding set of sources, whether they are negative or positive sign, and the ever changing magnitude of $|\vec{r} - \vec{r_i}|$. There is also an analogy between rays and images, for example take the middle plot of Fig. 1; the direct ray from source to receiver is the black path and surface-reflected ray generated by the image is the surface-reflected path.

To reach convergence in this example I needed about 80 images, although perhaps considerably fewer might suffice for an approximate solution. In contrast a simpler approach involves the method of normal modes (Fig. 2). From this figure one can tell that about 2 or 3 modes were needed. What are these modes?

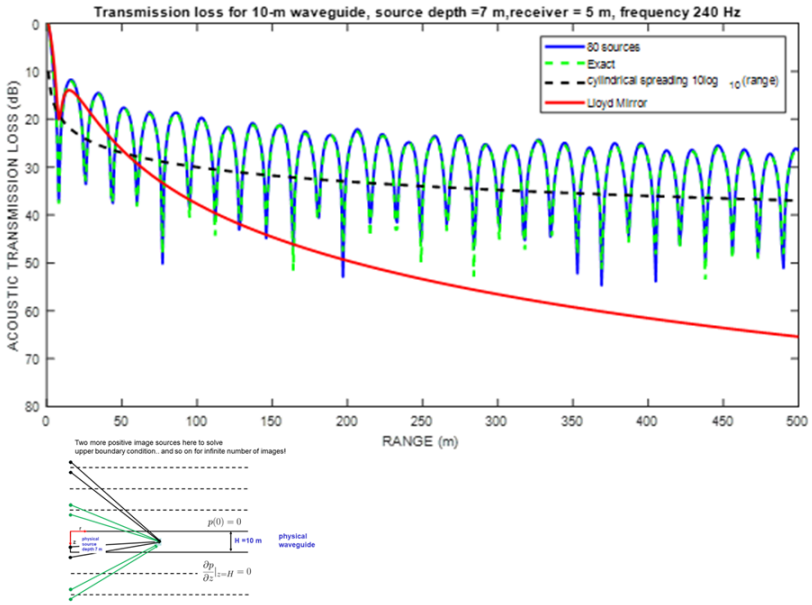

Figure 2: Comparison of image method of 80 images (blue line) and method of normal modes (green-dashed line) requiring 2 modes. Red line is Lloyd's mirror problem involving two images, and black-dashed line represents cylindrical spreading.

Before turning our attention to underwater waveguides, Fig. 3 shows the pressure distribution within a tube for which in one case (left side) the frequency f is such that $f < \frac{c}{1.7d}$ where d is tube diameter, and one axial mode is excited. This frequency f tube, diameter d, criterion was first discussed in Lectures 17 and 19 relating to the impedance tube and the single expansion chamber Muffler problems, rrespectively. Increasing the frequency (right side) produces excitation of more modes within the tube the single, axial mode approximation used to study the Muffler no longer applies.

We now focus on the underwater waveguide and an excellent experiment to understand modes

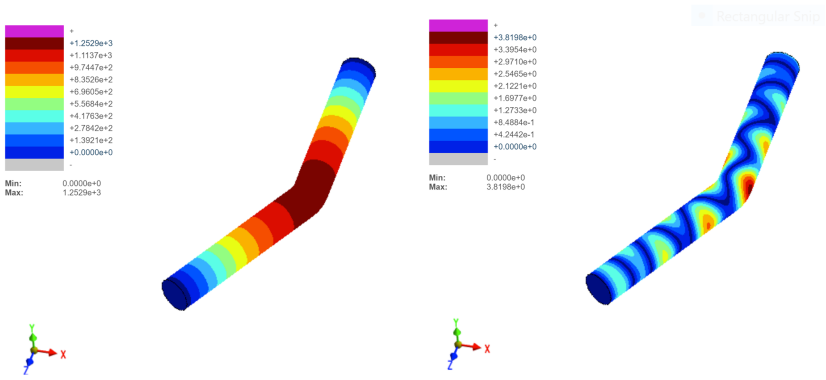

Figure 3: Left: pressure distribution within a bent tube frequency f is such that $f < \frac{c}{1.7d}$ where d is tube diameter; thus only one axial mode shown. Right: pressure distribution frequency $f > \frac{c}{1.7d}$ and several modes are excited.

in this environment comes from the study by Frisk, Lynch and Rajan (1989). Figure 4 shows the experimental geometry to measure mode in Nantucket sound. There are two acoustic receivers (hydrophones) on a buoy at depth 7.1 m and 12.5 m, and the average water depth is 14.6 m. An acoustic source suspended from a research vessel slowly moves away (opens in range) from these receivers, which are recording continuous wave (cw), or narrowband, sound at center frequency 140 Hz and 220 Hz. Thus, in terms of modeling of the receive sound the frequency content, and time dependence t. can be described with $e^{-i\omega t}$ where $\omega = 2\pi f$ and f is either 140 Hz or 220 Hz.

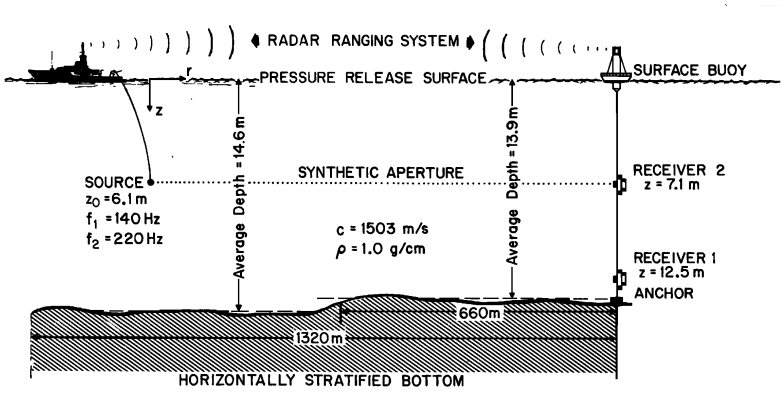

Figure 4: Geometry of experiment off Nantucket. Figure is Fig. 1 of Frisk, Lynch and Rajan (1989).

As the ship slowly opens in range from receivers which transmitting at these frequencies, modal interference patterns (Fig. 5) that depend on frequency and receiver depth, will be registered. One can tell right off that there about two modes in the interference pattern for 220 Hz shown in Fig. 5. Increasing the frequency well beyond 220 Hz will lead to a more complicated pattern owing to more than two modes, while decreasing the frequency substantially below 220 Hz will eventually yield just one mode. Lowering the frequency even further, say to about 100 Hz, then no modes are propagating: the *cutoff* frequency for this waveguide of depth about 15 m as been reached. This

estimate (with notation and form recast slightly) originates from (Frisk, 1994)

$$f_n = \frac{c_w}{2H}[\frac{n-1/2}{\sqrt{1-c_w^2/c_b^2}}] \tag{1}$$

where f_n is the cutoff frequency for the n^{th} mode, H is water depth, and c_w, c_b are water and seabed sound speeds, respectively. Using $H = 14.6$ m and typical values for c_w, c_b, find $f_n \sim 100$ Hz applies to the case of $n = 1$.

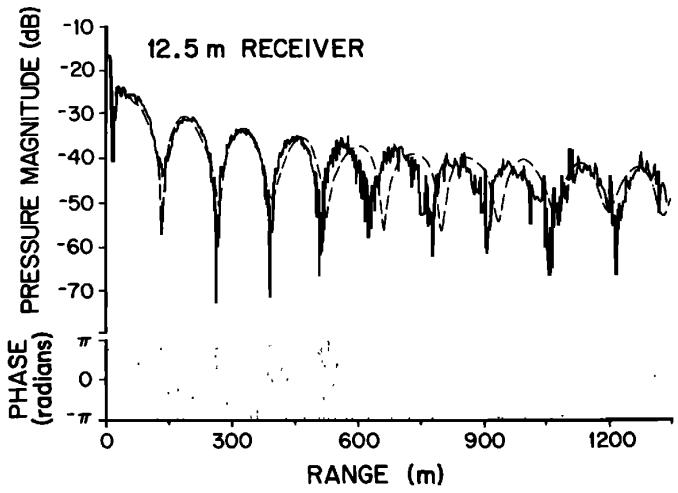

Figure 5: Transmission loss data for frequency 220 Hz, measured at depth 12.5 m versus range from source. Figure constitutes a portion of Fig. 3 of Frisk, Lynch and Rajan (1989). (The on-line version of the figure does not reproduce phase variation for this 1989 publication.)

The similarity between the simple model demonstration in Fig. 2 and the real data in Fig. 5 should be clear, both representing about two modes, and both showing an interference pattern with deep nulls, where the level of acoustic field drops precipitously then rises again. But some caution is needed to understand the obvious differences in notation between Figs. 2 and 5. In Fig. 2, a Green's function $g(z, r; z_0)$ is computed as function of range r, receiver depth z and source depth z_0, e.g., using both the method images (80 image case) and method of normal modes (2 modes). The plot is $-20\log_{10}\frac{|g(z,r;z_0)|}{|g(z,r=1\text{m};z_0)|}$, so the value at $r = 1$ m equals 0 dB; though highly oscillatory, upon increasing range r the field decays in strength, or more precisely in value of $|g(z, r; z_0)|^2$. Thus plotting $-20\log_{10}\frac{|g(z,r;z_0)|}{|g(z,r=1\text{m};z_0)|}$ yields a positive result. Such a plot is often referred to as "Transmission Loss" or TL and plotting in this manner gives the intuitive result of increasing TL with increasing range.

The Frisk *et al.* results appear as "Pressure magnitude" as in $-20\log_{10}|p|$, but also appear to be normalized in some manner, perhaps as $-20\log_{10}\frac{|p(12.5,r;6.1)|}{|p(12.5,r=1\text{m};6.1)|}$, where 12.5 and 6.1 represent the receiver and source depths, respectively. For example, in Fig. 5 the $|p|$ at range 500 m relative to $|p|$ at 1 m, appears to be about 30 to 40 dB less, which is not too different from Fig. 2 suggesting TL is

in about this range (just as a very rough comparison as frequencies).

The Method Normal Modes

The waveguide coordinate system (Fig. 6) is expressed in cylindrical coordinates (r, θ, z). There is symmetry in the θ direction, and the field is independent of θ; we need only to find the dependence in the r, z plane (white, dashed box in Fig. 2). The θ independence also means the final solution applies to any rotation about the $z-$ axis in Fig. 6. Thus the new problem involves the Laplacian operator in cylindrical coordinates without dependence on θ

$$\nabla^2 = \frac{1}{r}\frac{\partial}{\partial r}(r\frac{\partial}{\partial r}) + \frac{\partial^2}{\partial z^2}. \tag{2}$$

and we seek a new Green's function which satisfies the inhomogeneous Helmholtz equation for a point source at $z = z_s$ and $r = 0$

$$(\nabla^2 + k^2)g(r, z, z_s) = -2\frac{\delta(r)}{r}\delta(z - z_s). \tag{3}$$

The delta function expression on the right is different from the one we encountered previously. Here it represents a point source at source located at $z = z_s$ and $r = 0$ in cylindrical coordinates (Frisk, 1994, Kinsler *et al.*, 1980).

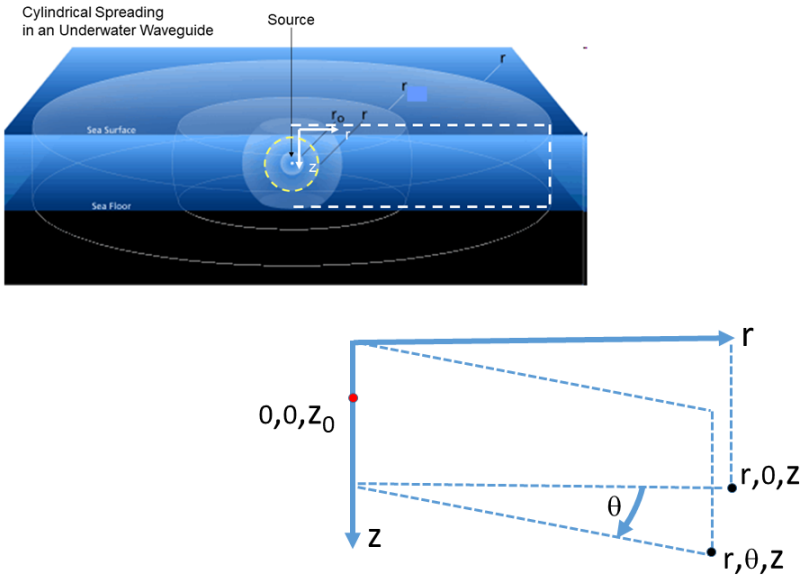

Figure 6: Cylindrical coordinate system for solving the wave equation in a waveguide. A source point (red) is located at depth z_0 with $r = 0$, and two receiver points (black) located at r, θ, z and $r, 0, z$. The analysis assumes no dependence in the θ direction.

Equation (3) is separable, meaning separate solutions for range $R_n(r)$ and depth $U_n(z)$ are found and multiplied together for solution in r, z. In doing so, multiple solutions corresponding modes will be found, where for example, $U_n(z)$ corresponds to the n^{th} mode. These are summed for the final solution

$$g(r, z, z_s) = \sum_n R_n(r) U_n(z). \tag{4}$$

The key effort involves finding the solution for the depth or z-dependent part, $U_n(z)$ which is responsible for satisfying the boundary conditions at the $z = 0, H$

$$(\frac{\partial^2}{\partial z^2} + \gamma_n^2) U_n = 0. \tag{5}$$

Equation (5) is a familiar 1D wave equation (Helmholtz equation) along the depth dimension z, although here the wavenumber k first seen in the Helmholtz equation, is replaced by its vertical component, where $\gamma_n^2 = k^2 - k_{rn}^2$. The vertical γ_n and radial or horizontal k_{rn} components of the wavenumber k vary according to mode number n but always satisfy $\gamma_n^2 + k_{rn}^2 = k^2$.

This is relation is depicted in Fig. 7 and one can imagine, approximately, that a high order mode (large n) corresponds to a ray with high grazing angle (steep ray) and low order mode (small n) corresponds to ray with shallow angle. This approximate correspondence between modes and rays is useful to keep in mind.

Underwater waveguide modes $U_n(z)$, analogous to modes of vibration of a guitar string, are functions that satisfy the boundary conditions in this case at the end points $z = 0$ and $z = H$. As in the guitar string, there can be many modes satisfying the boundary conditions; for the guitar string the boundary condition is that the string is clamped at both ends and therefore does not vibrate at those points. For the waveguide case, the surface and bottom boundary conditions are solved with $U_n(z) = A_n \sin(\gamma_n z)$ where $\gamma_n = \frac{(n-1/2)\pi}{H}$, and A_n is a normalization constant (discussed later). Note: the boundary condition was expressed in the form of pressure. The modes are not of dimension pressure *per se* but they are proportional pressure, or surrogate for pressure as in the Green's function. Thus if the $U_n(z)$ satisfy the boundary conditions, so too does pressure.

The first three modes $n = 1, 3$ (Fig. 8) for the underwater waveguide with same (idealized) boundary conditions used in Fig. 2, are shown frequency of 240 Hz and depth 10 m. One might call these mode functions, or eigenfunctions; observe that these functions all equal 0 at $z = 0$, and the vertical derivative equals 0 at $z = H$. A key property: the correspondence between mode number n and the number of times the mode function equals 0 over the depth span, or *zero-crossings*. The modes in this example appear to be some fraction of a sin wave, which in fact they are provided the sound speed within the water column does not change. This is a simplifying, but often realistic, assumption particularly in very shallow water as in Nantucket case where water sound speed is taken as a constant 1503 m/s. In deeper water, e.g., see Figs. 3 and 7 (Munk profile) of Lecture 21,

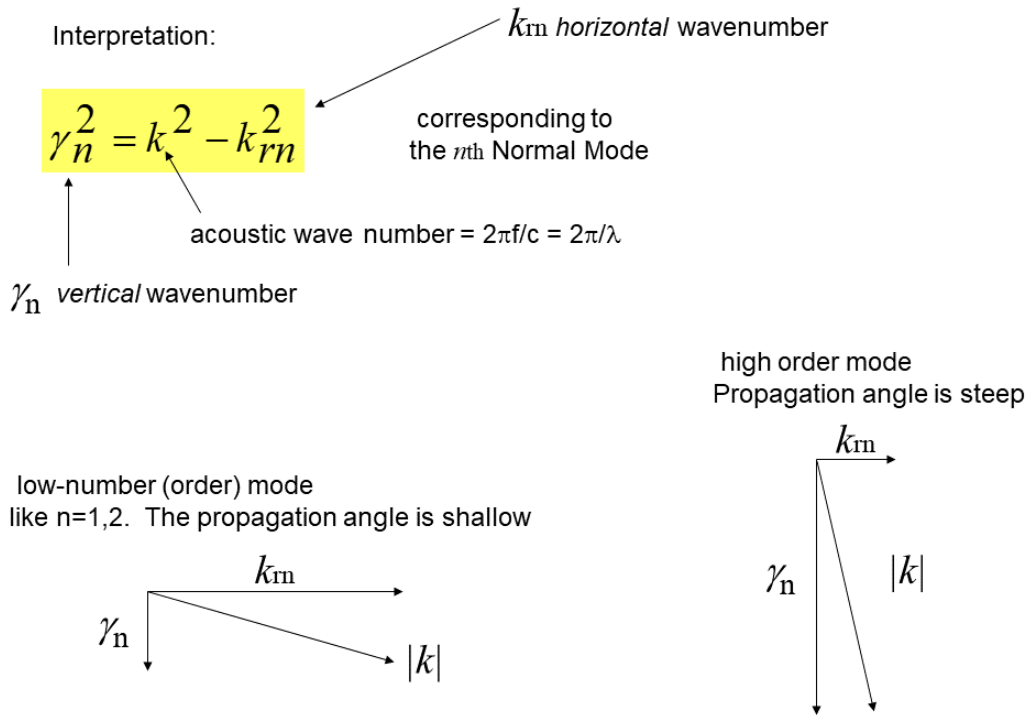

Figure 7: Interpretation of the wavenumber k in terms of its vertical γ_n and horizontal k_{rn} components.

variation in sound speed with depth changes the mode function shape which must be determined numerically.

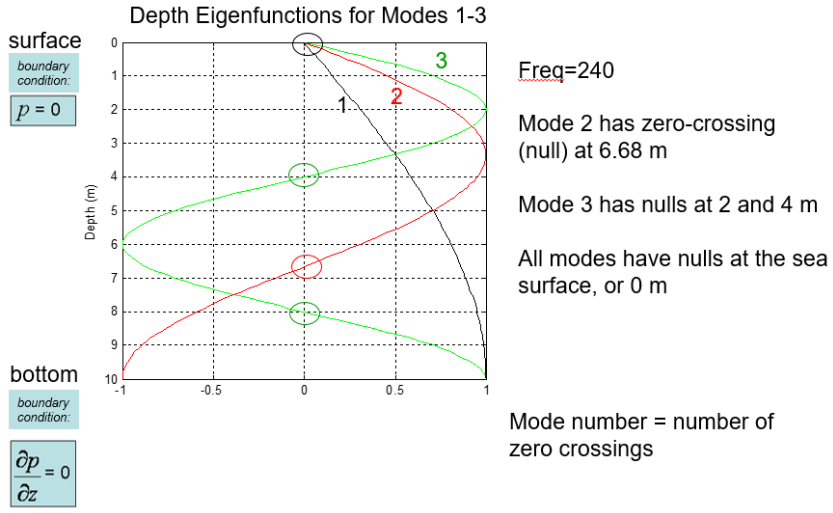

Figure 8: Eigenfunctions, or mode functions, for the first three modes for the case of frequency 240 Hz, depth 10 m. All modes have a zero-crossing at the surface, at $z = 0$, which constitutes the only zero-crossing for mode 1.

Looking ahead to the next lecture the final solution is

$$g(r, z, z_s) = \frac{2\pi i}{H} \sum_n \sin(\gamma_n z) \sin(\gamma_n z_s) H_0^1(k_{rn} r) \tag{6}$$

where H_0^1 is the zeroth-order Hankel function of the first kind, and is a member of the cylindrical Bessel family. Note the dimension for the Green's function $g(r, z, z_s)$ is L^{-1} (spherically spreading) just as with the free-space Green's function and method of images. However upon combining all these modes (or combining all those images in the method of images), we get a solution for pressure in the underwater waveguide that somewhat magically translates to pressure $\sim 1\sqrt{(}r)$ where r is range from source.

References

Frisk, G. V. *Ocean and Seabed Acoustics* (Prentice Hall, Englewood Cliffs, NJ, 1994)
Frisk, G. V., J. Lynch and S. Rajan, "Determination of the compressional wave speed profiles using modal inverse techniques in a range-dependent environment in Nantucket sound," *J. Acoust. Soc. Am.* 86, Nov. 1989.
L. E. Kinsler, A. R. Frey, A. B. Coppens, and J. V. Sanders, *Fundamentals of Acoustics*, (John Wiley & Sons, New York, 1980)

ME525 Applied Acoustics Lecture 24, Winter 2024
Method of Normal Modes

Peter H. Dahl, University of Washington

Details on the Green's function g derived from the Method of Normal Modes

The goal is to find a Green's function, g that satisfies the inhomogeneous Helmholtz equation for a point source at $z = z_s$ and $r = 0$

$$(\nabla^2 + k^2)g(r, z, z_s) = -2\frac{\delta(r)}{r}\delta(z - z_s). \tag{1}$$

The structure of the delta function in Eq. (1) applies to a cylindrical coordinate system (Fig. 1). The equation is separable into its r-dependent and z-dependent parts, and now we find $g(r, z, z_s)$ in terms of the sum of mode functions $U_n(z)$ multiplied by the corresponding $R_n(r)$, as in

$$g(r, z, z_s) = \sum_n R_n(r)U_n(z). \tag{2}$$

This yields a considerably useful and flexible solution approach.

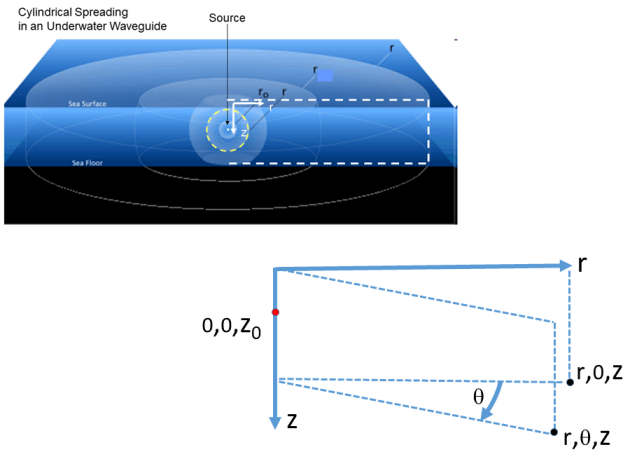

Figure 1: Cylindrical coordinate system for solving the wave equation in an underwater waveguide. A source point (red) is located at depth z_0 with $r = 0$, and two receiver points (black) located at r, θ, z and $r, 0, z$. The analysis assumes no dependence in the θ direction.

The radial part $R_n(r)$ has only one boundary condition known as the Sommerfeld radiation condition (e.g., see Frisk, 1994). For example, the radial dependence is not unlike ripples on water surface produced byh point disturbancance (as in dropping a rock), with the waves becoming more planar like the greater the range r from the source point on the surface.

It is with the vertical part where the surface and bottom boundary conditions are addressed, and the key effort reduces to finding the solution for the depth or z-dependent part, $U_n(z)$ to

$$(\frac{\partial^2}{\partial z^2} + \gamma_n^2)U_n = 0. \tag{3}$$

along with satisfying boundary conditions at the $z = 0, H$. The wavenumber k in Eq.(1) is broken up in vertical γ_n and horizontal k_{rn} components that vary according to mode number n and always satisfy $\gamma_n^2 + k_{rn}^2 = k^2$.

Equation (3) should be familiar problems of vibration and simple oscillations; $U_n(z)$ takes the form $\sin(\gamma_n z)$. We find γ_n via the eigenvalue equation

$$\gamma_n = \frac{(n - 1/2)\pi}{H}, \tag{4}$$

such that boundary conditions are satisfied. For example, $U_n = \sin(\gamma_n z)$ thus $U_n\Big|_{z=0}, \frac{\partial U_n}{\partial z}\Big|_{z=H} = 0$ for $n = 1, 2, 3....$ Equation (4) represents the most elementary of eigenvalue equations that is solvable exactly without numerical means. The situation is made more complicated when a real seabed with sound speed c_b and density ρ_b are added to the picture.

Orthonormality of mode functions U_n

An important property of U_n is that this function be orthonormal such that integral over depth is

$$\int_0^H U_n U_m dz = \delta_{nm} \tag{5}$$

where δ_{nm} is the Kronecker delta symbol which equals 1 for $m = n$ and 0 for $m \neq n$. For certain this integral equals 0 for for $m \neq n$, but to equal 1 when $m = n$ a normalization constant A_n is needed given $U_n(z) = A_n \sin(\gamma_n z)$. This requirement puts the normalization rcnstant A_n equal to $\sqrt{\frac{2}{H}}$. For this simple case with the waveguide boundary conditions are such that $U_n\Big|_{z=0}, \frac{\partial U_n}{\partial z}\Big|_{z=H} = 0$ the normalization constant A_n is the same for all modes, but in general there will be a dependence on mode number n.

Details on the radial dependence $R_n(r)$

The next step represents a traditional approach for solving partial differential equations that are separable (it is worthwhile revisiting these steps on your own) . First insert Eq.(2) as candidate solution to Eq. (1) yielding

$$\sum_n \nabla^2 R_n(r)U_n(z) + k^2 R_n(r)U_n(z) = -2\frac{\delta(r)}{r}\delta(z - z_0) \tag{6}$$

Now break up the $\nabla^2 = \frac{1}{r}\frac{\partial}{\partial r}(r\frac{\partial}{\partial r}) + \frac{\partial^2}{\partial z^2}$ operator into r and z dependencies. Exploit Eq. (3), along with important relation $k^2 = k_{rn}^2 + \gamma_n^2$ to arrive at:

$$\sum_n U_n \frac{1}{r}\frac{\partial}{\partial r}(r\frac{\partial R_n}{\partial r}) + R_n k_{rn}^2 U_n = -2\frac{\delta(r)}{r}\delta(z - z_s). \tag{7}$$

The separation constant and split of the partial differential equation into r and z dependencies was key. Adapt this language for consistency with Fig. 7 of Lecture 23: k_{rn}^2 is the *horizontal wavenumber* for the n^{th} mode; γ_n^2 is the *vertical wavenumber* for the n^{th} mode.

Now multiply both sides of Eq.(7) by U_m and integrate over depth z from 0 to H, and invoke the *orthonormal property* along with the *sifting property* of the delta function, to yield

$$\frac{1}{r}\frac{\partial}{\partial r}(r\frac{\partial R_m}{\partial r}) + R_m k_{rm}^2 = -2\frac{\delta(r)}{r}U_m(z_s) \tag{8}$$

The above represents a purely radial form of the Helmholtz equation with point source at origin $r = 0$ (e.g. somewhat akin to ripples on the surface of a pond, the pond being of infinite extent) but multiplied by the constant $U_m(z_s)$ since the source depth z_s is a fixed value. (The change from k_{rn} to k_{rm} being of no significance, merely a result of our choosing to go with U_m.)

The solution is well-known and solved by functions of the cylindrical Bessel family, in this case the zeroth-order Hankel function of the first kind which we denote as H_0^1. The solution for index n is

$$R_n(r) = i\pi H_0^1(k_{rn}r)U_n(z_s) \tag{9}$$

where $U_n(z_s)$ provides the dependency on source depth needed for the Green's function.

Type "help besselh" in Matlab to obtain more information about H_0^1. In Matlab evaluate $H_0^1(k_{rn}r)$ as besselh$(0, 1, k_{rn} * r)$, where r is vector of ranges and k_{rn} is horizontal wavenumber for the n^{th} mode. A useful approximation for $H_0^1(k_{rn}r)$ is

$$H_0^1(k_{rn}r) \approx \sqrt{\frac{2}{\pi}}e^{-i\pi/4}\frac{e^{ik_{rn}r}}{\sqrt{k_{rn}r}} \tag{10}$$

Though strictly valid for $k_{rn}r >> 1$ is often used in underwater acoustic modeling computations for computational simplicity.

The final solution is thus

$$g(r, z, z_s) = \frac{2\pi i}{H}\sum_n \sin(\gamma_n z)\sin(\gamma_n z_s)H_0^1(k_{rn}r) \tag{11}$$

Notice that the basic dimension for the Green's function $g(r, z, z_s)$ is L^{-1}, owing to the $1/H$ dependence out front, but the behavior for far ranges is $\sim 1/\sqrt{r}$ which can be more clearly seen in the

asymptotic expression of Eq. (10).

The number of modes and cut-off frequency

Given the important behavior more apparent in Eq. (10) of $\frac{e^{ik_{rn}r}}{\sqrt{k_{rn}r}}$, it should be clear that if k_{rn} becomes imaginary to any significant degree, that mode will not go very far. For example, take the waveguide examined previously (Fig. 2) with frequency 240 Hz, $H = 10$ and water sound speed 1450 m/s. Run through Eq.(4) starting from $n = 1$ and compute the corresponding k_{rn}, get:

Table 1: Modes for waveguide of $H = 10$ m, frequency 240 Hz, $c_w = 1450$ m/s, and $k = 1.04$ m^{-1}

Mode number	γ_n	k_{rn}	**Will this mode propagate?**
1	0.15713	1.0280	yes
2	0.4712	0.9271	yes
3	0.7854	0.6817	yes
4	1.0996	i 0.357	no

Obviously the vertical wavenumber continues to grow with increasing mode number, and once it exceeds the wavenumber in the water column k then, k_{rn} becomes imaginary. Note: which imaginary do we take from the square root, the positive or negative? In ME 525 with $e^{-i\omega t}$ dependence, you *must* take the positive square root to make Eq.(10) work properly. So, clearly the number of modes in this example is three, or it is said there are three *trapped* modes in this waveguide.

However, Fig. 2 takes on the appearance closer to two trapped modes, given the regular interference pattern, rather than three inferred from Table 1. Revisit Fig. 8 from Lecture 23 where U_n is plotted for these three modes. The source depth, 7 m, was very close to the zero crossing of mode 2, hence this mode was weakly excited.

Indeed taking advantage of mode zero crossings in terms of placement of source and receiver depths is done in experiments. Figure 3 represents such an example where a source (frequency 43 Hz) is towed at depth 45 m in waters of depth 77 m off the coast of New England (about 100 km south of Cape Cod). The measured water sound speed profile and assumed model for the seabed are each shown in the left of the figure–clearly these vary from the simplifications of having a constant water velocity and rigid seabed. Yet the modes (solid lines, right figure) assume a quasi-sinusoidal dependence. With source placed at depth 45 m, mode 2 (red, solid line) is only weakly excited since this depth is close to zero crossing at about 50 m. Data (and modeling) from this experimental configuration (Fig. 4) clearly show a more simple 2-mode interference pattern.

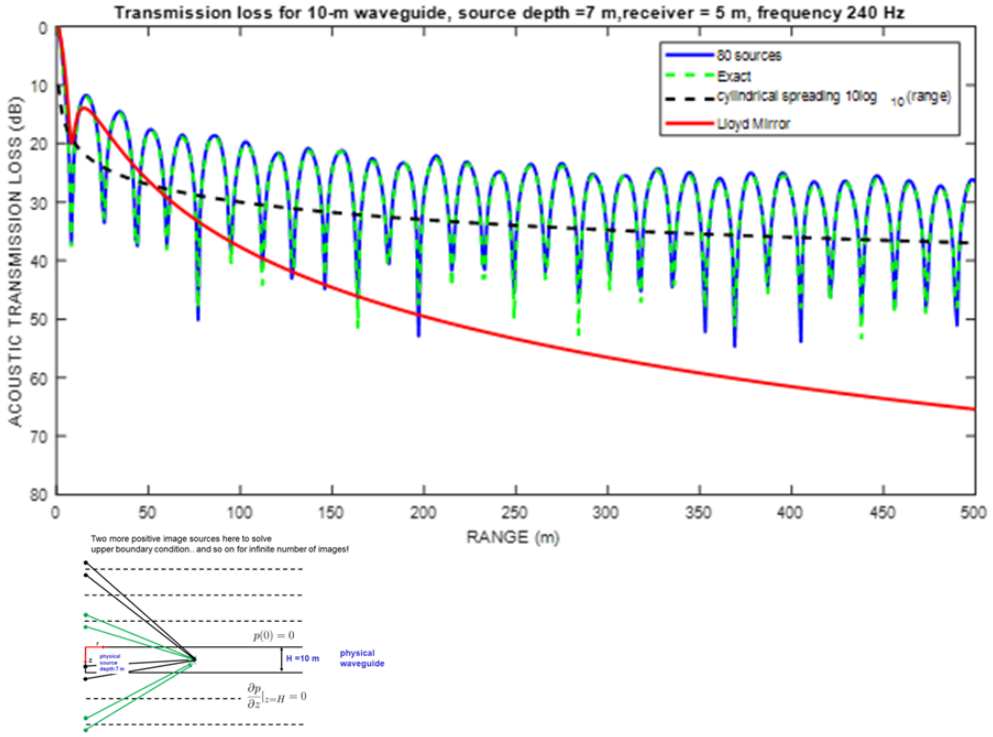

Figure 2: Upper: comparison of 80 image-source result with the method of normal modes. Lower: Layout for method of images based on sources of the form e^{ikR}/R where R depends on image location. Depth $H = 10$ m

Examine next a case for depth H equal to 100 m (Fig. 5), where Eq. (10) now gives exactly 33 trapped modes before an imaginary k_{rn} emerges. Interestingly we can also reasonably approximate the solution with far fewer image sources, e.g., about 8 image sources (and even the simple Lloyd mirror solution consisting of just two image sources provides reasonable approximation up to ranges of about 50 m). Given we were able to liken image sources to the concept of an acoustic ray, these two examples illustrate an interesting trade off: when the acoustic field in the waveguide requires many modes to fully describe it, then typically it can be described with much fewer rays, and vice versa. It will no doubt pay in your research to keep this trade off in mind.

The number of modes in a waveguide of depth H depends on the sound frequency, or more precisely the sound wavelength λ, with a simple and useful rule of thumb for this number being

$$n_{modes} \approx 2H/\lambda \tag{12}$$

For this example of $H = 10$ m, n_{modes} is 3.2, for $H = 100$ m, there 10 times the number of modes.

Keep in mind Eq.(12) is the simplest of rules, which will need to be modified for more realistic boundary conditions at the seabed that involve finite sound speed and density for sediment, for example, refer to Fig. 1 of Lecture 18. We can compute the corresponding discrete horizontal angle

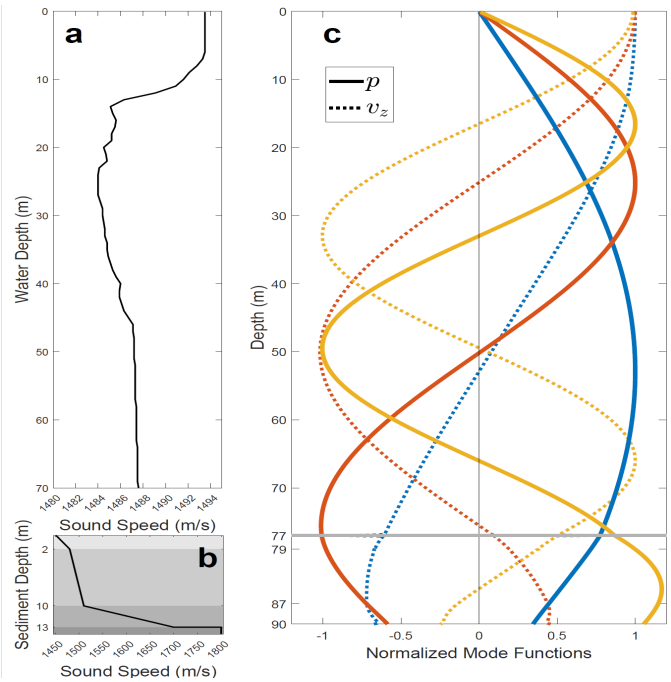

Figure 3: Left: sound speed profile (measured) and seabed model used to compute mode functions (right) at frequency 43 Hz using the computation program ORCA. Modes functions of discussion are solid lines. Corresponding dashed lines represent modes for the vertical component of acoustic velocity based on the vertical derivative of the solid lines. Notice that mode 2 (red, solid line) goes through a zero crossing near 50 m. Figure from Dahl, Dall'Osto and Hodgkiss, 2023.

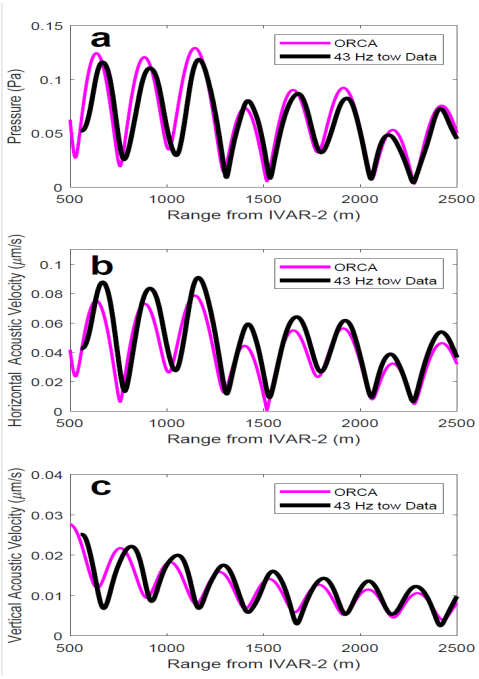

Figure 4: (a) Acoustic pressure (b) horizontal velocity and (c) vertical velocity at 43 Hz over the towing range of 500 to 2500 m from the receiver. Measured data (black) and modeled data (magenta) based on the ORCA program. Figure from Dahl, Dall'Osto and Hodgkiss, 2023.

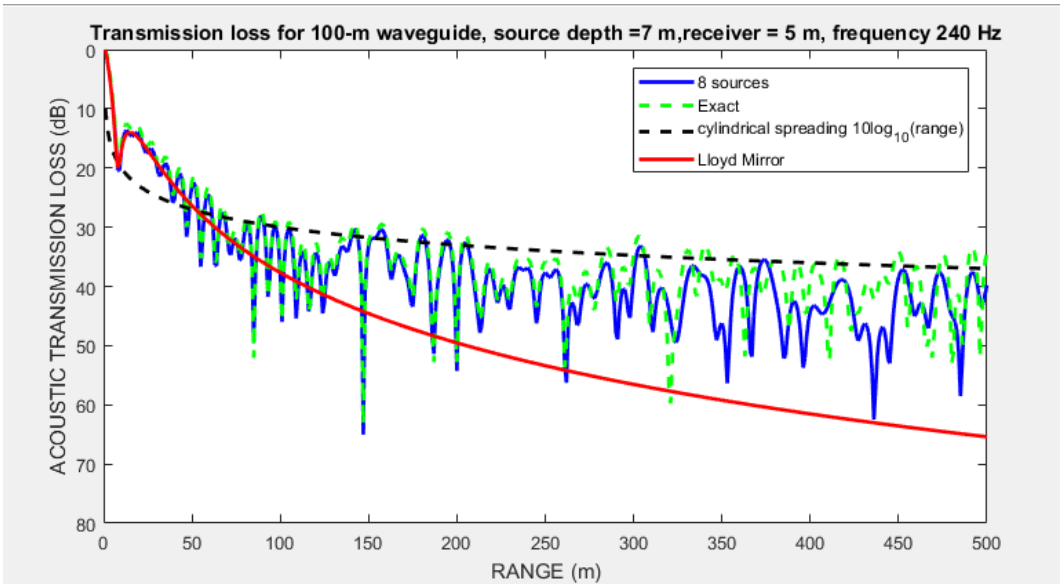

Figure 5: Acoustic transmission loss for waveguide with same boundary conditions, source frequency, and source/receiver depth as in Fig. 2, but with depth $H = 100$ m.

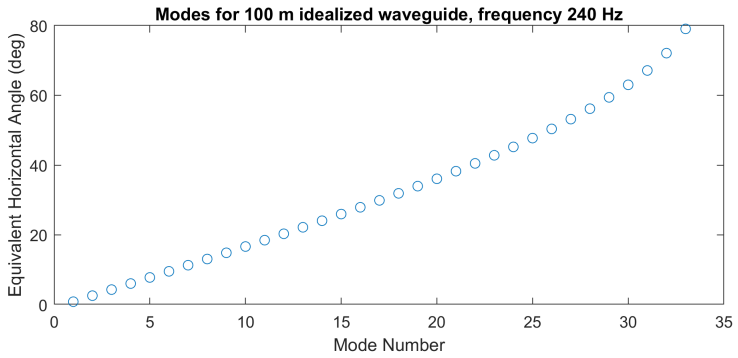

Figure 6: The discrete set of horizontal mode angles for the 33 trapped modes for the waveguide in Fig. 3, but with depth $H = 100$ m.

call it θ_n for each of the 33 trapped modes for the 100-m case (Fig. 6), where $k_{rn} = \cos\theta_n k$. These angle get quite steep for the high mode numbers, getting to about 80°. But, in the more realistic case θ_n must be $\leq \theta_c$.

References

Frisk, G. V. *Ocean and Seabed Acoustics* (Prentice Hall, Englewood Cliffs, NJ, 1994)
P. H. Dahl, D. R. Dall'Osto and W.S Hodgkiss, "Active intensity vortex and stagnation point singularities in a shallow underwater waveguide," *J. Acoust. Soc. Am.* 154, Sep 2023.

ME525 Applied Acoustics Lecture 25, Winter 2024
Normal modes in more realistic waveguides
The depth-dependent Green's function

Peter H. Dahl, University of Washington

As shown in Lecture 24, there are is a corresponding discrete horizontal angle, θ_n, for each of n-trapped modes computed, defined as $k_{rn} = \cos\theta_n k$. It is useful to view each mode as having a propagation angle, or a "specific preferred direction of propagation" for that mode (Frisk, 1994). The $\cos$ of this angle relative to horizontal equals k_{rn}/k.

The sequence of discrete angles continues to increase starting from mode-1 (see Fig. 6 of Lecture 24) until no more propagating modes are found–the point at which k_{rn} becomes imaginary. Placement of an imaginary k_{rn} into the argument of $H_0^1(k_{rn}r)$ produces rapid, exponential decay as a function range r– easier to see in the asymptotic expression H_0^1. Such modes are known as evanescent modes.

The simple model for boundary conditions at $z = 0, H$ (Fig. 1, upper) is useful because it exhibits properties of the *discrete angular spectrum* associated with trapped modes. However this rigid boundary condition on the seabed does not permit a critical angle–the assumption being that the sound speed in the seabed is infinite, and the boundary represents an *infinite impedance boundary*. With presence of a critical angle, there is a more interesting transition between trapped modes and those with higher mode numbers. The problem is made considerably more realistic (Fig. 1, lower) without too much more effort by including the plane wave reflection coefficient R representing reflection at the boundary between an upper (water) medium with sound speed c_1 and a lower (sediment) medium with sound speed c_2. From our earlier study of R we found that a critical angle θ_c is defined at $\cos\theta_c = c_1/c_2$.

The critical angle provides the demarcation (Fig. 2) between discrete angular spectrum (trapped modes) with propagation angles $< \theta_c$, and the continuous angular spectrum with propagation angles $> \theta_c$. The discrete set of preferred propagation angles (blue rays) is within the yellow cone defined by the critical angle, outside of which is the continuous set of propagation angles (red rays) that can exist at a continuos range of angles all greater than θ_c. Rays corresponding to the continuous set exist only close to the source (within about one or two water depths) because their contribution is quickly attenuated due to energy loss from propagation into the seabed. An approximate range after which the contribution is primarity from the discrete, trapped modes is $\sim \frac{H}{\tan\theta c}$, or about twice the value of R_o in Fig. 2.

Modes in a realistic waveguide

Upon using a realistic sound speed and density in the seabed, the boundary becomes a *finite*

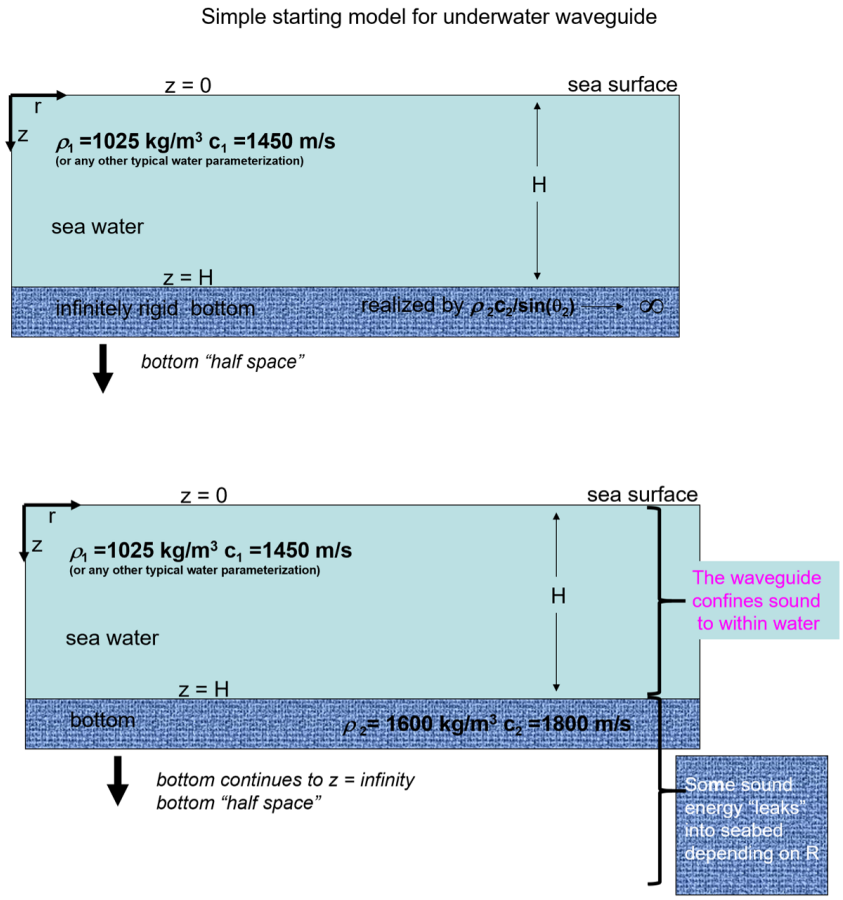

Figure 1: Upper: Idealized waveguide we have been studying with boundary conditions at $z = 0, H$, and solution given by Eq.(2). Lower: more realistic waveguide for which the plane reflection coefficient R describes the boundary condition at $z = H$.

impedance boundary, as described by R. The new equation for solving for γ_n is

$$1 + Re^{2i\gamma_n H} = 0 \tag{1}$$

where R is also a function γ_n. Quick check: put $R = 1$ corresponding to the infinite impedance boundary and recover the original specification for $\gamma_n = \frac{(n-1/2)\pi}{H}$. However, Eq.(3) as defined is a transcendental equation that does not have closed-form solution. Instead numerical approaches, such as Newton Raphson, can be used to find the zeros of Eq.(3) as function of γ_n.

Without much numerical effort we get a quick visualization on where the modes are located by plotting $|1 + Re^{2i\gamma_n H}|$ over a fine angular resolution (Fig. 3). Although this is not a recommended approach to finding the zeros of an equation it is immediately apparent where modes are located. In this example, water sound speed $c_1 = 1525$ m/s, sediment sound speed $c_2 = 1700$ m/s, water density $\rho_1 = 1024$ kg/m^3 and seabed density $\rho_1 = 1800$ kg/m^3, with quantities sufficient to specify the plane wave reflection coefficient R. To identify specific modes both a water depth are required,

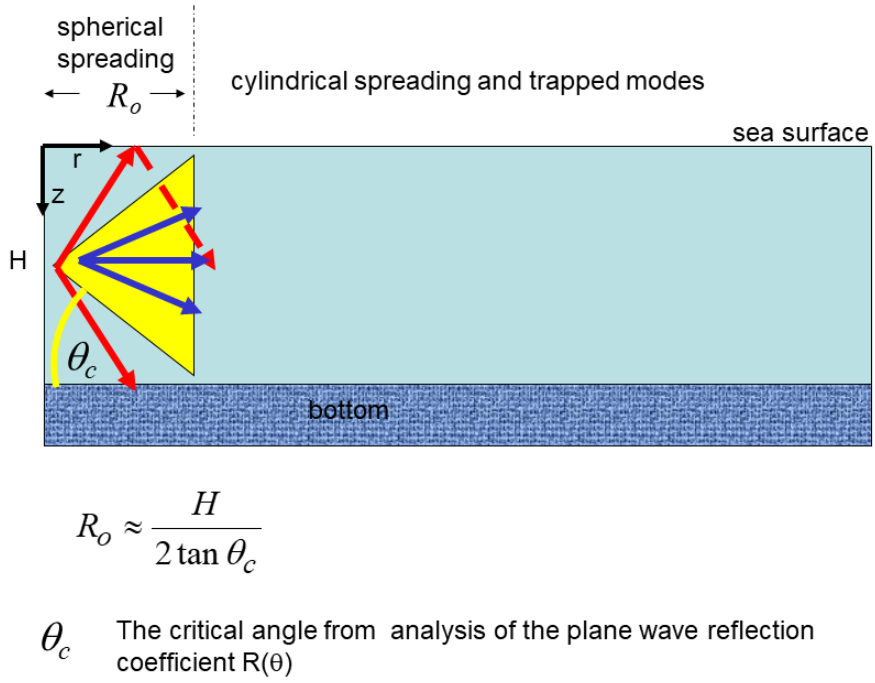

Figure 2: Idealization depicting the discrete set of preferred propagation angles (blue rays) within the yellow cone as defined by the critical angle, and the continuous set of propagation angles (red rays) that can exist *angle* angles greater than θ_c.

for this example H = 50 m and frequency= 200 Hz. The reflection coefficient (remaining fully complex) is computed over a fine grid of grazing angles θ (Fig. 3 upper). For every θ, a $\gamma = k_1 \sin\theta$ is identified, i.e., a continuous range of γ as distinct from a discrete set, such as γ_n. A plot of $|1+Re^{2i\gamma_n H}|$ (Fig. 3 lower) shows a set of minima, representing the discrete set of propagation angles for this waveguide. These angles (shown by the circles) are: 3.9920°, 8.0270°, 12.1400°, 16.3500°, 20.668°, and 25.0530°, values that are likely as close as one can get with a numerical approach. Note that the critical angle, $26.22°$ is greater than largest angle in the discrete set and effectively bounds these angles.

To summarize, the discrete angles –"preferred propagation angles" – of the trapped modes all must be less than critical angle. The modes are trapped, and will efficiently propagate within the waveguide with little if any attenuation, as can be anticipated by observing that $|R| \approx 1$ for angles less than critical. Efficient propagation is also inferred from corresponding horizontal wavenumber for trapped modes k_{rn} which primarily real-valued. There can be a small imaginary component in k_{rn} to account for attenuation effects within the seabed. Ultimately, solutions to Eq.(1) are found for angles greater than the critical angle θ_c These modes belong to the realm of the continuous spectrum of angles, where the steep propagation angles lead to penetration into the seabed and

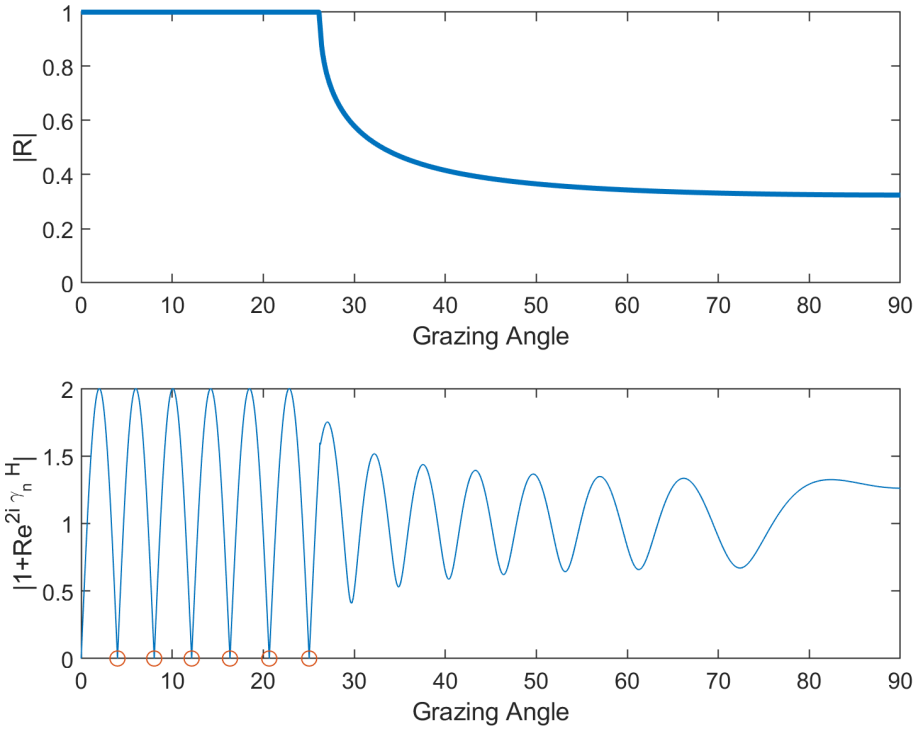

Figure 3: Upper: magnitude of the reflection coefficient $|R|$. Lower: L $|1 + Re^{2i\gamma_n H}|$ over a fine angular resolution. The six minima to the left of the critical angle at 26.22° are trapped modes (not counting the first minimum), and are identified by circles.

significant energy loss with increasing range.

Here is very handy formula for the approximate number of trapped modes in realistic underwater waveguide

$$\texttt{Number trapped modes = floor}(\frac{k_1 H}{\pi}\sin\theta_c + \frac{1}{2}) \tag{2}$$

which, upon applying the waveguide parameters discussed in Fig. 3, predicts the 6 modes.

The field in a realistic waveguide

As reminder the solution studied thus far for the Green's function applied to a waveguide depth of H, with boundary conditions $g|_{z=0} = 0$ and $\frac{\partial g}{\partial z}|_{z=H} = 0$, infinite impedance case for the seabed, which is

$$g(r, z, z_s) = \frac{2\pi i}{H}\sum_n \sin(\gamma_n z)\sin(\gamma_n z_s)H_0^1(k_{rn}r) \tag{3}$$

Upon inclusion of a finite impedance seabed the new set of discrete vertical γ_n or the equivalent horizontal k_{rn} mode wavenumbers, e.g., via Eq. (1), and the mode normalization constant is (Frisk,

Eq. (5.144))

$$A_n = \sqrt{2}[\frac{1}{\rho_1}(H - \frac{\sin 2\gamma_n H}{2\gamma_n}) + \frac{1}{\rho_2}\frac{\sin^2 \gamma_n H}{\gamma_{2n}}]^{-1/2}. \tag{4}$$

Compare with constant $A_n = \sqrt{\frac{2}{H}}$ for the infinite impedance case.

The revised Green's function finite impedance seabed becomes

$$g(r, z, z_s) = \frac{\pi i}{\rho_1} \sum_n A_n^2 \sin(\gamma_n z) \sin(\gamma_n z_s) H_0^1(k_{rn} r). \tag{5}$$

Continuing with the example discussed in Fig. 3, to properly implement Eq.(4) we also need a vertical wavenumber in the lower (seabed) medium, call it γ_{2n}. This is found via

$$\sin \theta_{2n} = i\sqrt{(\frac{c_2}{c_1} \cos \theta_n)^2 - 1} \tag{6}$$

Then γ_{2n} equals $k_2 \sin \theta_{2n}$ where it is understood that $k_2 = \frac{\omega}{c_2}$. But since all θ_n are by definition less than the critical angle, then $\sin \theta_{2n}$ is imaginary resulting in exponential decay in the field in the lower medium for $z > H$.

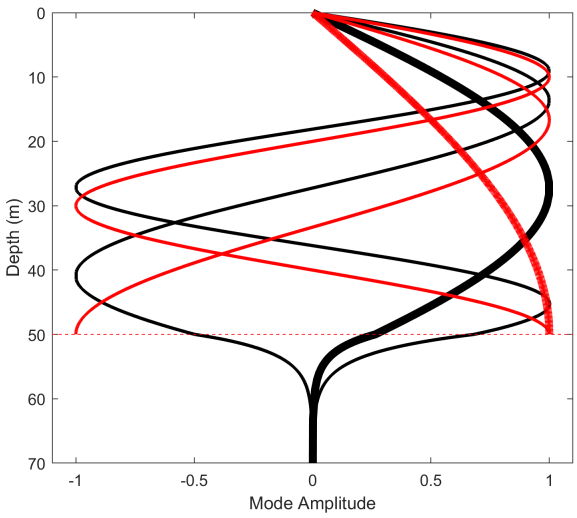

Figure 4: Mode functions for the first three modes finite impedance boundary under discussion in Fig. 3 of this lecture (black lines) compared infinite impedance case (red lines). Mode 1 for each case is plotted with thicker line. Note that for infinite impedance case the mode functions cannot extend below the boundary at depth 50 m.

Examine carefully the mode functions for the first three modes associated with finite impedance boundary case under study (Fig. 4), and compared with equivalent mode functions for the *infinite* impedance case. With finite impedance case, there is exponential decay into the seabed for depths greater than 50 m (refer to Frisk, Eq. (5.145) for how to compute the mode functions there). For this

example it appears that modes 2 and 3 are not too different from the simplified infinite impedance boundary example, but mode 1 shows a substantial difference. The Green's function as defined by Eq. (5), with A_n given by Eq.(4) is actively used in underwater acoustics research today; it describes what is known as the Pekeris waveguide, named after the physicist C. L. Pekeris (1908-1993).

The depth-dependent Green's function for a Pekeris waveguide

The following is a brief of introduction meant to give additional perspective on the Green's function for an underwater waveguide with cylindrical symmetry, as summarized by the modal summations formulas in Lecture 25; these in the form of Eq. (3), representing rigid (infinite impedance) boundary condition on the seabed and Eq.(5) representing finite impedance condition separating water and seabed halfspace, or the Pekeris waveguide. The perspective originates from examining these functions with a completely equivalent representation based on the Hankel transform of a depth-dependent Green's function (Frisk, 1994).

The depth-dependent Green's function for the Pekeris case (Frisk, 1994, Eq. 6.64) is

$$g(k_r) = \frac{i(e^{i\gamma|z-z_s|} - e^{i\gamma(z+z_s)} + Re^{2i\gamma H}(e^{-i\gamma(z+z_s)} - e^{-i\gamma|z-z_s|}))}{\gamma(1 + Re^{2i\gamma H})}. \tag{7}$$

Things to notice: (i) the variable range r is missing, (ii) there remains the depth variable z, and constant for source depth z_s, (iii) the mode horizontal wave number k_{rn} and vertical γ_n are missing the indices n and appear to assume continuous distribution of values, and, importantly, (iv) the denominator should look familiar where R is the reflection coefficient of the seabed.

The field is recovered via a Hankel transform of $g(k_r)$ over the continuous distribution of horizontal wavenumbers k_r, yielding

$$g(r, z, z_s) = \int_0^\infty g(k_r) J_0(k_r r) dk_r \tag{8}$$

where J_0 is the 0^{th} order Bessel function. The Hankel transform is transforming from wavenumber domain, k_r, to a spatial domain in terms of range r, akin to Fourier transform with time and frequency.

As an example take the Pekeris waveguide (Fig. 1, lower) with water speed $c_w = 1450$m/s, sediment speed $c_b = 1800$ m/s and water depth $H = 20$ m. For frequency 220 Hz this waveguide looks to support about 3 trapped modes according to Eq.(2) of Lecture 25.

The Hankel transform must undertake a contour integral in the complex k_r-plane (Fig. 5) where a discrete set of poles, or singularities, each yield a residue contribution giving back the same solution we discussed previously involving a mode sum. The poles are located at discrete locations k_{rn}, with the figure depicting three such poles.

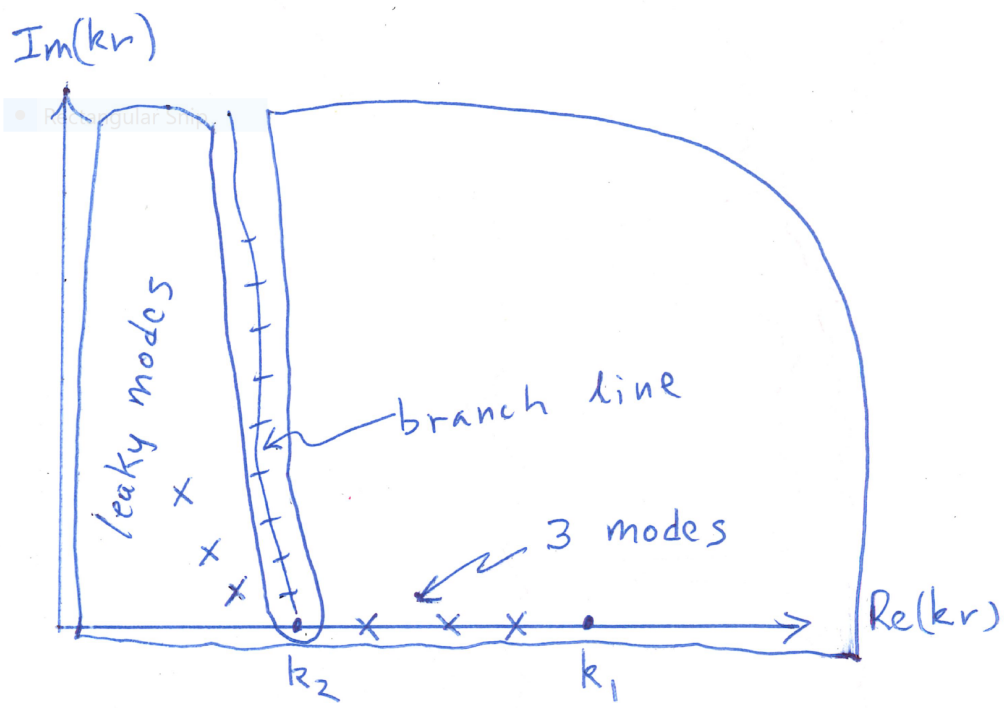

Figure 5: Sketch of the location of three trapped modes $k_{rn} n = 1, 2, 3$ located on the real-kr axis between wavenumbers k_1 (water layer) and k_2 seabed. A branch point is located at k_2, and to further to the left are a few leaky modes described by increasing imaginary part of the modal wavenumber. An integration contour is shown within which poles are located.

At the point on the complex k_r-plane located at k_2 there exists a *branch point* singularity. Here a choice must be made given the square-root ambiguity for $k_r = \pm k_2$. We choose $+k_2$ in accordance with our convention of $e^{-i\omega t}$ and this prevents the integral from being unbounded and becoming infinite. But this choice necessitates a branch line integral along the contour shown in the figure. Notice: the branch point corresponds to the critical angle.

There are approximate, asymptotic solutions to the branch line integral (Frisk, 1994), otherwise numerical approaches are needed. Often the contribution of branch line integral is just ignored–just as it has in the solutions we've been discussing thus far consisting of a discrete modal summation. This is because it represents the continuum of angles $\theta > \theta_c$, where such "equivalent" rays undergo significant reduction in amplitude upon each interaction with the seabed causing rapid attenuation with increasing range from the source.

One clever way to deal with this branch line contribution to the integral is to recast the branch line singularity into a set of modes with increasing imaginary component, known as "leaky modes" as they leak energy into the seabed and rapidly attenuate. One of my favorite approaches is that of Zang and Tindle (1993) who capture this effect in their mode-finding algorithm, and these modes can thus included in a modal summation. They are referred to as "imperfect resonances" or "improper modes" (Frisk, 1994); in contrast, one should think of a trapped mode as a complete or

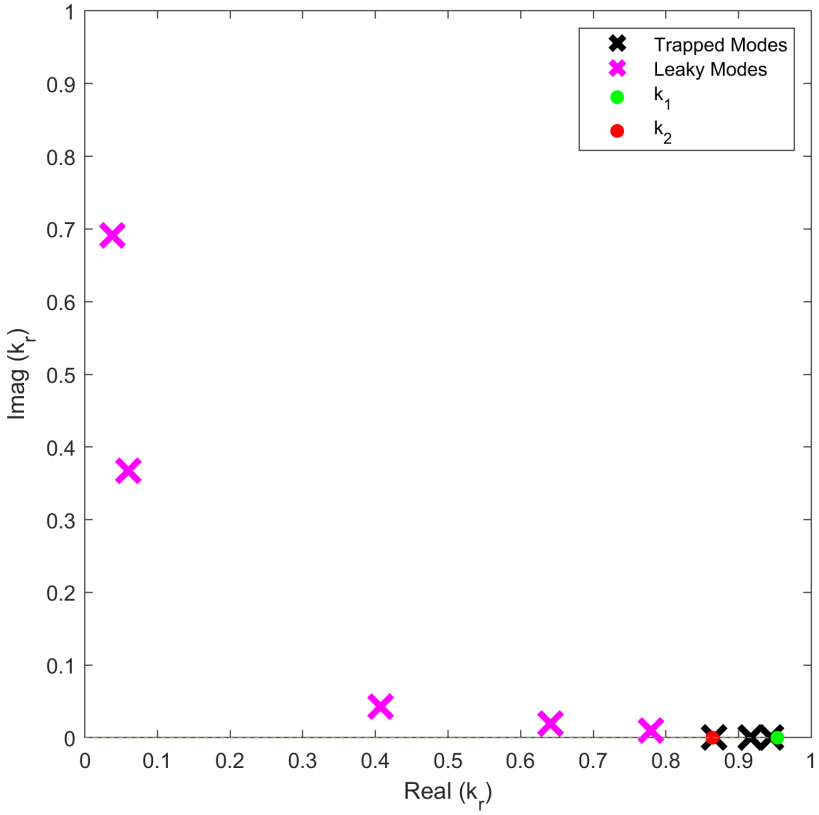

Figure 6: Plot of k_r in complex plane for frequency is 220 Hz corresponding to the Pekeris waveguide of Fig. 1, but with c_b = 1600 m/s. The waveguide supports about three trapped modes that are located between k_1 and k_2. Some leaky modes exist, with increasing imaginary component.

perfect resonance of the waveguide. A map of complex k_r plane (Fig. 6) shows the three trapped and four leaky modes along with their relation to the wavenumbers k_1 and k_2. There are many more leaky modes than the four shown–but the fourth one is a goner anyway, given its huge imaginary component, and probably only the first two leaky modes to the left of the branch point at k_2 make any meaningful contribution.

Figure 7 shows results of a computation involving both trapped plus leaky modes for the waveguide similar to Fig. 1 (lower), with frequency 220 Hz, but c_b = 1600 m/s giving a critical angle of 25° for c_w = 1450 m/s. Roughly, b range 40 to 50 m, the situation is fully described by the three trapped modes. Find $\sim \frac{H}{\tan\theta c} \sim 43$ m, which reasonably describes a range delineating the transition from continuous + discrete modes to discrete, or trapped, modes.

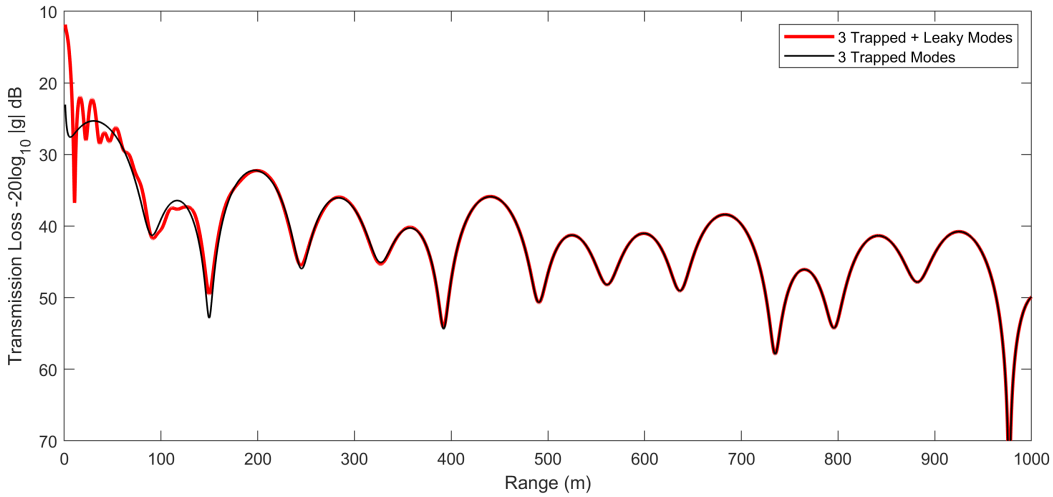

Figure 7: Pekeris waveguide. At a frequency of 220 Hz, this waveguide supports about three trapped modes.

References

Frisk, G. V. *Ocean and Seabed Acoustics* (Prentice Hall, Englewood Cliffs, NJ, 1994)

Z. Y. Zang, and C. Tindle, "Complex effective depth of the ocean bottom" *J. Acoust. Soc. Am.* 93,205-213, 1993